VOL. 10, NO 20, NOVEMBER, 2015 ISSN 1819-6608
ARPN Journal of Engineering and Applied Sciences

www.arpnjournals.com

OPTIMIZED FSI FLOW SIMULATION USING MODERN UP-TO-DATE SOFTWARE SYSTEMS: A DIRECT COMPARISON BETWEEN SIMULATED AND TUNNEL RESULTS

Luca Piancastelli[1], Leonardo Frizziero[1], Giampiero Donnici[1], G. Di Giacomo[1] and A. Gattii[2]
[1]Alma Mater Studiorum University of Bologna, Department of Industrial Engineering, Viale Risorgimento, Bologna, Italy
[2]Alenia Aermacchi - A Finmeccanica Company, Piazza Monte Grappa, Rome, Italy
E-Mail: leonardo.frizziero@unibo.it

ABSTRACT

The goal of this study is the analysis of the CFD/FSI simulation accuracy of complex shapes with standard CAD-embedded software packages. In a PLM (Product Lifecycle Management) system, the continuous improvement of CAD-embedded FSI (Fluid System Interaction) software packages has progressively reduced the necessity for highly specialized external partners. These simulation software packages are designed to keep pace with the unavoidable design development. To make FSI and CFD usable for mechanical designers and design engineers from other engineering disciplines, CFD software package have been largely automated. The specialist expertise required to operate traditional CFD software may be negligible However, the capabilities of CAD-embedded CFD to handle complex geometries and to simulate complex industrial turbulent flows with heat and mass transfer raise question of the accuracy on the results obtainable by a non-specialized designer. In this paper, a paraglider wing from NASA TN D3442 was used as a case study. This wing was modelled inside commercial CAD software and then thoroughly analysed by using the simulation tools with their default settings. The accuracy of results was then evaluated.

Keywords: CFD, FEA, FSI, paraglider wing.

INTRODUCTION

High quality, complete and accurate CAD 3D models are the starting point for all virtual prototyping and physical simulations. These data form the bulk of the Product Lifecycle Management (PLM) that is widely deployed by many industries. PLM is the tool by which 3D manufactured product data are used and maintained during an entire product's lifecycle and across all its design changes.

The combined use of Computational Fluid Dynamics, (CFD) and FE (Finite Element) in CAD-centred system can significantly accelerate the design process. However, this process may have a drawback of increasing design complexity. This fact unavoidably increases the dependence on external "specialized" development partners for simulation and optimization. The continuous improvement of CAD-embedded FSI (Fluid System Interaction) software packages has progressively reduced the necessity for these external partners. These software packages are designed to keep pace with the unavoidable design development. Engineering simulations, interpretations and optimizations follow the geometry changes. To make FSI usable for mechanical designers and design engineers from other engineering disciplines, CFD software package have been largely automated to minimize the specialist expertise required to operate traditional CFD software. The capabilities of CAD-embedded CFD to handle fairly complex geometries and also to simulate complex industrial turbulent flows with heat and mass transfer is then extremely important, together with simulation's turbulence capabilities.

In this paper, a paraglider wing from NASA TN D-3442 was used as a case study. This wing was modelled inside commercial CAD software and then thoroughly analysed by using the simulation tools with their default settings. The accuracy of results was then evaluated and thoroughly analysed.

BRIEF NOTES ON THE CFD CODE

Nowadays, even our CAD-embedded Flow Simulation software is a 10 years old mature code with thousand person-years of development effort behind it [1]. It utilizes a modified k-ϵ two-equation turbulence model optimized for a wide range of turbulence scenarios. An immersed boundary Cartesian meshing techniques allow for accurate flow field resolution with low cell mesh densities [2] (Figure-1).

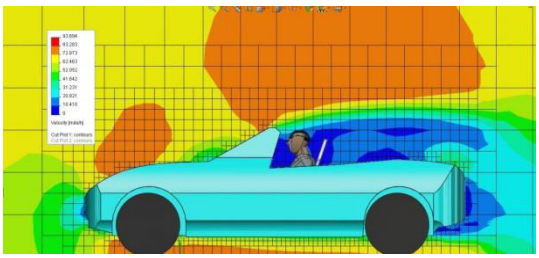

Figure-1. Immersed boundary cartesian mesh [3].

The immersed boundary methods are simple. At first, the pre-processor detects the computational cells that are cut by the body. The cells are then divided in those that are inside and outside of the body.

The cut cells are separated in two types of cells corresponding to the location of their cell center. The cells that have their geometrical centre outside or on the surface of the body are labeled as interface cells. The other cut cells are treated like inside cells.

The flow variable φ, which represents a turbulence variable, is set to zero in the inside cells.

At the interface cells, the nearby wall is modeled with an off wall boundary condition, which in general consists of a linear interpolation pattern corrected with a (non-linear) correction.

The scalar variable φ in the interface cell *(i,j)* is interpolated in two steps, using only the neighboring cells that are further away from the body. Initially, a linear interpolation is carried out along the normal to the wall up to an intermediate location that has the same distance to the wall as the interface cell center *(i,j)* for each neighboring cell. The second interpolation takes on a surface that is parallel to the wall. Here, the inverse-distance weighted method proposed by Franke (1982) [4] that preserve local maxima and produces smooth reconstructions. The interpolation of φ(i,j) in the interface cell is:

$$\varphi_{(i,j)} = \sum_m \frac{w_m \varphi_m}{q} \quad (1)$$

With

$$w_m = \left(\frac{H - h_m}{H \times h_m} \right)^2 \quad (2)$$

And

$$q = \sum_m w_m, m = \{N, S, E, W\} \quad (3)$$

where φ_m are the previously interpolated values, h_m is the distance between the position of φ(i,j) and the position of φ_m and H is the maximum of the values of h_m.

The sum is over the neighboring cells, with m that identify the cell over (N-Nord), under (S-South) on the left (E-East) and on the right (W-West) of the current cell. The weights w_m=0 for all non-qualifying neighbors. For each interface cell the described linear interpolation results in a set of weights β_m which summarize the effect of each neighbor cells on the interface cell:

$$\varphi_{(i,j)} = \beta_W \varphi_W + \beta_E \varphi_E + \beta_S \varphi_S + \beta_S \varphi_S \quad (4)$$

By considering only the neighboring cells (W, E, S, N) that have a common face with the interface cell (i, j) the linear interpolation (4) can easily be treated in an implicit way. In fact, in the computational CFD RANS (Reynolds Averaged Navier-Stokes) code, a second-order, implicit, cell centered Cartesian mesh is used within a pressure-velocity coupling algorithm with a segregated solution of the field equations [5]. These equations are discretized in three-dimensions with a 7-point pattern. However, in this brief introduction, we will refer for simplicity to the corresponding two-dimensional equations. Therefore, for each cell (i,j), the discretized field equation for momentum, turbulent scalar and pressure correction can be written as:

$$a_W^n \varphi_W^{n+1} + a_E^n \varphi_E^{n+1} + a_s^n \varphi_s^{n+1} + a_N^n \varphi_N^{n+1} = s_{(i,j)}^n \quad (5)$$

The implicit matrix of the equation (5) can be modified with the weights β_m without introducing new diagonals with non-zero elements. However, the inclusion of geometrical singular points such as corners should be done explicitly. For a non-linear near wall behavior of φ an explicit correction $\Delta\varphi_{corr}$ is added to the right hand side of equation (4). This mesh generator can be used in conjunction with Van Driest's (1956) universal profiles. These profiles can be used to describe two classes of turbulent boundary layers. The thick boundary layer model is used when the fluid mass centers of the near-wall mesh cells are located inside the boundary layer. The thin boundary layer model substitutes the first one when the fluid mass centers of the near-wall mesh cells are located outside the boundary layer. These boundary layer models overcome the problem of a very fine mesh density near the walls in the calculation. The Launder Spalding functions specify the wall boundary conditions for the RANS in an enhanced turbulence k-ϵ model. In the other regions of the computational domain the k-ϵ with damping model of Lamand Bremhorst [6] describes laminar, turbulent, and transitional flows of homogeneous fluids consisting of turbulence energy conservation equations (6) (7).

$$\frac{\partial \rho k}{\partial t} + \frac{\partial \rho k u_i}{\partial x_i} = \frac{\partial}{\partial x}((\mu + \frac{\mu}{\sigma_k})\frac{\partial k}{\partial x_i} + \tau_{ij}^R \frac{\partial u_i}{\partial x_j} - \rho\varepsilon + \mu_t P_B \quad (6)$$

$$\frac{\partial \rho \varepsilon}{\partial t} + \frac{\partial \rho \varepsilon u_i}{\partial x_i} = \frac{\partial}{\partial x}((\mu + \frac{\mu}{\sigma_k})\frac{\partial \varepsilon}{\partial x_i} + C_{\varepsilon 1}\frac{\varepsilon}{k}\left(f_1 \tau_{ij}^R \frac{\partial u_i}{\partial x_j} + {}_{\varepsilon 1}\mu_t P_B \right) - f_2 C_{\varepsilon 2}\frac{\rho \varepsilon^2}{k} \quad (7)$$

With

$$\tau_{i,j} = \mu s_{ij},\ \tau^{R}_{i,j} = \mu_i s_{ij} - \frac{2}{3}\rho_k \delta_{ij},\ s_{ij} = \frac{\partial u_i}{\partial x_i} + \frac{\partial u_j}{\partial x_j} - \frac{2}{3}\delta_{ij}\frac{\partial u}{\partial x_k},$$

$$P_B = -\frac{g_i}{\sigma_B \rho}\frac{\partial \rho}{\partial x_i}$$

where C_{ij}=0.09, C_{t1}=1.44, C_{t2}=1.92, σ_k=1, σ_ε=1.3, σ_B=0.9 and C_B=1 or C_B=0 for P_B>0 and P_B<0.

Lam and Brembhorst's damping function are used in the turbulent viscosity term (8) (9).

$$f_\mu = \left(1 - e^{-0.025R_y}\right)^2 \left(1 + \frac{20.5}{R_t}\right) \quad (8)$$

$$\mu_t = f_\mu \left(\frac{C_\mu \rho k^3}{\varepsilon}\right) \quad (9)$$

y is the distance of the point from the wall, and

$$R_y = -\frac{\rho y \sqrt{k}}{\mu}, R_t = -\frac{\rho k^2}{\mu \varepsilon}$$

Lam and Bremhorst's damping functions fμ, f_1, f_2 decrease turbulent viscosity and turbulence energy and increase the turbulence dissipation rate. These parameters are controlled by the Reynolds number R_y. R_y is calculated on the average velocity of fluctuations and distance from the wall. When f_μ= 1, f_1 = 1, f_2 = 1 the approach obtains the original k-ε model.

A fluid's boundary layer requires a very high-density mesh to give accurate results. This approach impairs the computational efficiency of the simulation and usually requires long computer time on extremely performing computing systems. For this reason, the computational mesh used in our CFD code is always an immersive boundary non-body-fitted Cartesian mesh. For this purpose, the dimensionless distance parameter from the wall parameter y^+ is used (10).

$$y^+ = \frac{y\sqrt{\tau_w k}}{\mu} \quad (10)$$

Therefore, the dimensionless distance from the turbulent equilibrium region's outer boundary up to y^+=300 follows the experimental data presented by Wilcox (1994) [7]. With this approach, the CFD explicitly obtains the momentum, heat flux, and turbulent boundary conditions for the RANS. This approach simplifies the mesh and reduces the computational time even in large domains. It is then possible to obtain accurate results with standard desktop computers.

Flexible wing simulation

The first step of any FSI simulation is to verify that the data obtained with the software are reliable. In particular, it is important to understand, whether the result are acceptable with the default settings. This fact is important for two different aspects. The less important is the possibility for nearly all the users to access to the simulation results. The most important is that, with CFD codes, the level of knowledge of the domain and of the theory embedded in the software requires extremely qualified operators. Specific training may be required to optimize the simulation, if the software is not able to take care of most of the problems. Another very important aspect is the computer resources necessary to obtain reliable results. If supercomputers are needed the result are beyond the possibility of most users. This fact is true also for large Companies were the high speed computing systems are always overbooked. For this purpose, a simulation was carried out on a relatively complex wing of known geometry. Highly reliable experimental data are available for the configuration considered.

Therefore, the paraglider configuration having a large tapered leading edges and keel of NASA tn D-3442 was considered ideal for the FSI simulation accuracy test.

For a paraglider configuration having large inflatable tapered leading edges and keel, NASA made low-subsonic wind-tunnel and free-flight. These extremely expensive experimental tests and the geometry of the paraglider are fully documented in the paper. Wind-tunnel tests indicated that this wing configuration had a maximum lift-drag ratio of approximately 3.0 and positive static longitudinal and lateral stability. The flight tests validated the wind tunnel work and demonstrated that the configuration could be trimmed for steady gliding flight and was capable of recovering the capsule from launches at zero speed at extreme pitch and roll attitudes.

The NASA designed to be used as a parachute for the return of space capsules is shown in Figures 2 and 3.

Figure-2. Original wind tunnel photograph from the wind tunnel tests [NASA tn D-3442].

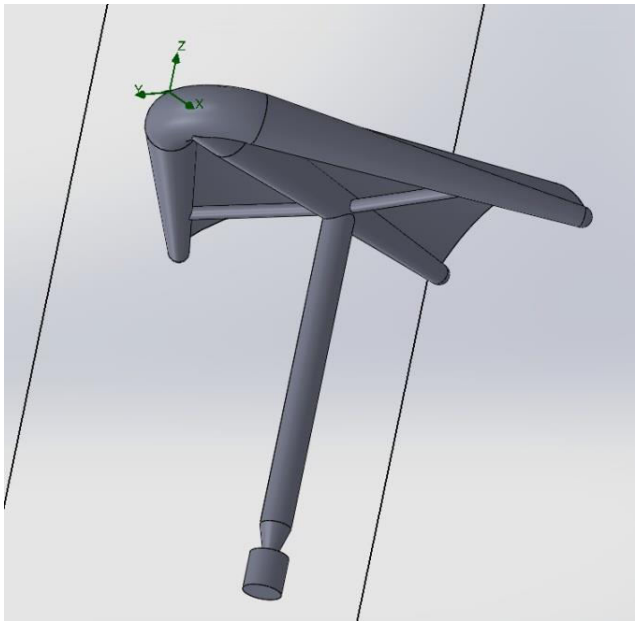

Figure-3. FSI deformed model.

For the FSI model the inflated part of the wing was considered rigid. The elastic wing canopy was made of stabilized Dacron^{TM} sailcloth weighing 166 g/m^2. Only the canopy was then considered deformable. As we will see later, this assumption is probably the reason of the difference from the simulated and the true wing at extremely high angles of attack. The paraglider has been considered by the NASA Langley Research Center as a recovery system for booster rockets, manned spacecrafts returning from orbital and suborbital flights. Through several years of research, experimental and analytical investigations have been made to evaluate the capabilities of the paraglider as a recovery device

NASA explains that the present paraglider configuration considered in this paper was designed to investigate micrometeoroid impacts in space by using an instrumented flexible canopy which provided a relatively large sensor area that could be recovered after reentry. The paraglider was of an inflated tube construction to allow packaging in the launch vehicle and deployment in space. Static force tests to determine the aerodynamic characteristics of a 0.0472-scale model of the configuration were made at Mach number up to 4.5. However, these supersonic results are not used in this paper.

The present paper uses the data obtained by NASA tn D-3442 on the low-speed static aerodynamic characteristics and flight behavior of the paraglider configuration. NASA obtained the static aerodynamic characteristics on both a 1/5-scale for wind tunnel testing and a full-scale model; free-flight tests were made by an outdoor drop and uncontrolled glide technique with the full-scale model.

Simulation vs. Wind tunnel results

With our CFD software, it is possible to use different accuracy levels. The less precise results are obtained by relaxing the tolerance on the convergence parameters (goals). These latter are chosen by the operator. In our case, the goal was the velocity. The possibility to choose the accuracy levels made it possible to check for boundary conditions and mesh before running the final tests. This possibility saves operator time and costs, giving a direct "true" measure of the simulation time. Therefore, common mistakes in input data can be corrected before the final, time consuming run is performed. The values obtained by the FSI simulation proved to be reliable, but only up to AOA (Angle of Attack) of 40° with the software default settings (Figure-4 and Table-1). However, the accuracy of the initial CAD model proved to be critical. Several changes on the CAD had to be made to obtain satisfactory results.

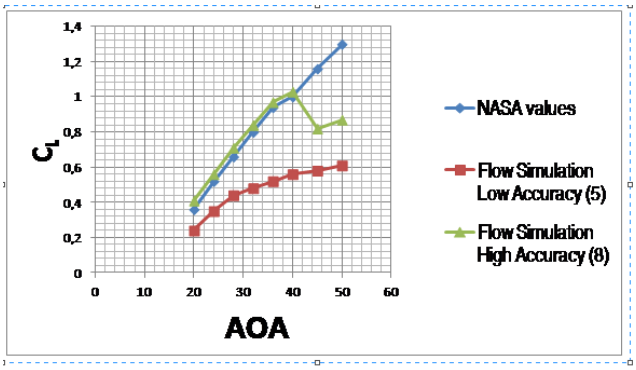

Figure-4. Simulated values (red=low accuracy, green=high accuracy) vs. NASA (blue).

It proved to be extremely important to take into account of the deformed shape of the canopy under the effect of aerodynamic loads (Figure-5).

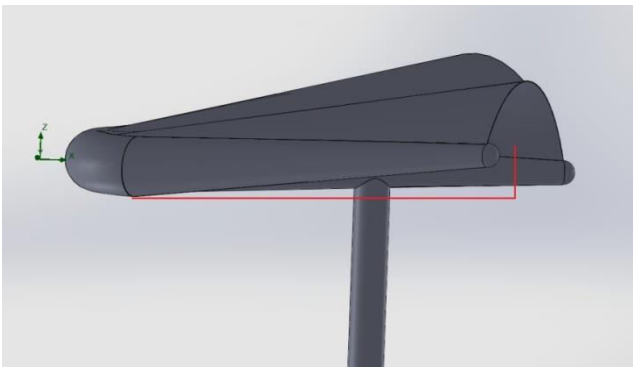

Figure-5. The canopy deformed by the aerodynamic loads (from the FE model).

Another extremely critical factor is to keep the canopy tangent to the inflated structure (Figure-6).

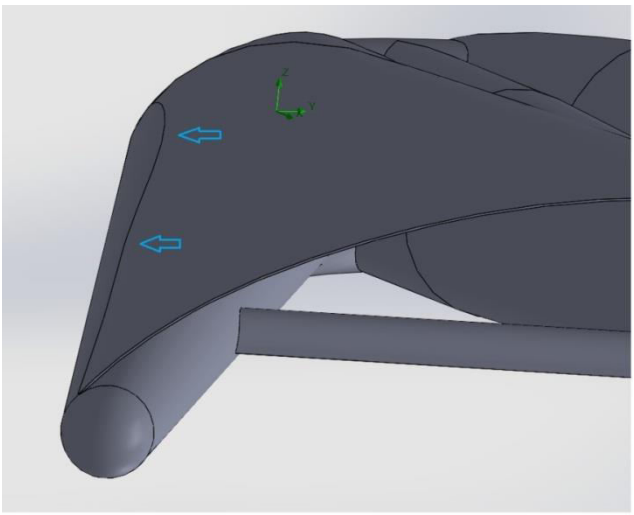

Figure-6. Canopy should be tangent to the inflated part of the wing.

The discrepancies of the results obtained for angles greater than 41are probably because the original wing is completely made of cloth. Therefore, it is flexible in all its parts and can deform in all points due to the actions of the loads aerodynamic. On the contrary, the inflated part of the wing was considered an entirely solid body. Hence, the inflated "structure" of the wing remains unchanged under the effect of loads.

Table-1. Experimental vs. CFD results.

AOA	Esperimentai	CFD low accuracy	CFD high accuracy
20°	0.36	0.32	0.41
24°	0.52	0.46	0.56
28°	0.66	0.58	0.71
32°	0.80	0.63	0.84
36°	0.94	0.68	0.97
40°	1	0.76	1.03

The influence of the Reynold number on the simulation

The results of Figure-4 and Table-1 were obtained with the original wind tunnel data, s.l. ISA+0 and 30.61 m/s. The same static aerodynamic characteristics were obtained on both a 1/5-scale and the full-scale CAD model. At this point, tests were carried out in different conditions of fluid speed on the full-scale model (30 m/s, 20m/s, 12m/s, ISA +0) without any significant variation in the C_L-AOA curve.

CONCLUSIONS

The goal of this study is the analysis of the CFD/FSI simulation accuracy of complex shapes with standard CAD-embedded software packages. In a PLM (Product Lifecycle Management) system, the continuous improvement of CAD-embedded FSI (Fluid System Interaction) software packages has progressively reduced the necessity for highly specialized external partners. These simulation software packages are designed to keep pace with the unavoidable design development. To make FSI and CFD usable for mechanical designers and design engineers from other engineering disciplines, CFD software package have been largely automated. The specialist expertise required to operate traditional CFD software may be negligible However, the capabilities of CAD-embedded CFD to handle complex geometries and also to simulate complex industrial turbulent flows with heat and mass transfer raise question of the accuracy on the results obtainable by a non-specialized designer. In this paper, a paraglider wing from NASA TN D-3442 was used as a case study. This wing was modelled inside commercial CAD software and then thoroughly analysed by using the simulation tools with their default settings. The accuracy of results was then evaluated. The results are extremely accurate up to 40° AOA (Angle Of Attack). Over this value, the flexibility of the wing structure and the turbulence requires an accurate tuning of the simulation parameters. However, the accuracy of the results in the usable field of the wing (under 40°AOA) is impressive. They were obtained with a commercial laptop with an extremely reasonable solution-time and without any specialised input from the designer.

Symbols

Symbol	Description	Unit
$\varphi_{(i,j)}$	Scalar variable linked to the tangential velocity for the cell i,j	-
w_m	Boolean weight to qualify the m= N,E,W,S neighbors	-
φ_m	Scalar variable linked to the tangential velocity for neighbors of cell i,j	
h_m	Distance between the centroids of cell i,j the neighbor cell m	m
p	Exponential factor for interpolation 1=linear	-
β_m	Weight of the neighbour cell on the cell i,j	-
$a_m\Phi_m$	Interpolation factors for momentum, turbulence scalar and pressure correction factors	-
n	Iteration number	-
s	Correction factor for for momentum, turbulence scalar and pressure correction factors	-
u_j	j-th component of the fluid velocity vector	m/s
ρ	Fluid density	kg/m^3
k	Turbulence energy	J/kg
ϵ	Dissipation rate of turbulence energy	W/kg
μ	Fluid viscosity	Pa s
$\tau_{i,j}$	ij-th component of laminar stress tensor	Pa
$\tau_{i,j}^R$	ij-th component of Reynolds stress tensor	Pa
P_r	Prandtl number	-
Pr_i	TurbulentPrandtl number	-
C_p	heat capacity under constant pressure	kJ/(kg K)
T	Temperature	K
x_j	j-th coordinate Cartesian system	m
n_j	j-th component of the normal to the wall in the fluid region	m
y	Distance from the wall along the normal to it	m
y^+	Dimensionless distance from the wall along the normal to it	-
k	Karman factor	-
A_v	Van Driest damping factor	-
δ	Boundary layer thickness	m

REFERENCES

[1] Gavriliouk V.N., Denisov O.P., Nakonechny V.P., Odintsov E.V., Sergienko A.A., Sobachkin A.A. 1993. Numerical Simulation of Working Processes in Rocket Engine Combustion Chamber. 44th Congress of the International Astronautical Federation, IAF-93-S.2.463, October 16-22, Graz, Austria.

[2] Kalitzin G. and Iaccarino G. 2002. Turbulence Modeling in an Immersed-Boundary RANS-Method, Center for Turbulence Research Annual Research Briefs, Stanford University, California. pp. 415-426.

[3] Shuvom G. 2011. Practical Flow Simulation at Highway Speeds, http://blog.capinc.com/2011/06/practical-flow-simulation-at-highway-speeds/.

[4] Franke, R. 1982. Scattered data interpolation: Tests of some methods. Math. Comput. 38, 181-200.

[5] Ferziger J. H. and Peric M. 2002 Computational Methods for Fluid Dynamics. Springer-Verlag, third-edition.

[6] Lam C.K.G. and Bremhorst K.A., 1981. Modified Form of Model for Predicting Wall Turbulence. ASME Journal of Fluids Engineering. 103: 456-460.

[7] Wilcox D.C. 1994. Turbulence Modeling for CFD. DCW Industries.

[8] L. Piancastelli, L. Frizziero, I. Rocchi, G. Zanuccoli, N.E. Daidzic. 2013. The "C-triplex" approach to design of CFRP transport-category airplane structures. International Journal of Heat and Technology, ISSN 0392-8764, 31(2): 51-59.

[9] L. Frizziero, I. Rocchi. 2013. New finite element analysis approach. Published by Pushpa Publishing House. Far East Journal of Electronics and Communications. ISSN: 0973-7006, 11(2): 85-100, Allahabad, India.

[10] L. Piancastelli, L. Frizziero, E. Pezzuti. 2014. Kers applications to aerospace diesel propulsion. Asian Research Publishing Network (ARPN). Journal of Engineering and Applied Sciences. ISSN 1819-6608, 9(5): 807-818, EBSCO Publishing, 10 Estes Street, P.O. Box 682, Ipswich, MA 01938, USA.

[11] L. Piancastelli, L. Frizziero, G. Donnici. 2014. A highly constrained geometric problem: The inside-outhuman-based approach for the automotive vehicles design. Asian Research Publishing Network (ARPN). Journal of Engineering and Applied Sciences. ISSN 1819-6608, 9(6): 901-906, EBSCO Publishing, 10 Estes Street, P.O. Box 682, Ipswich, MA 01938, USA.

[12] L. Frizziero, F. R. Curbastro. 2014. Innovative methodologies in mechanical design: QFD vs TRIZ to develop an innovative pressure control system. Asian Research Publishing Network (ARPN). Journal of Engineering and Applied Sciences. ISSN 1819-6608, 9(6): 966-970, 2014, EBSCO Publishing, 10 Estes Street, P.O. Box 682, Ipswich, MA 01938, USA.

[13] L. Piancastelli, L. Frizziero. 2014. How to adopt innovative design in a sportscar factory. Asian Research Publishing Network (ARPN). Journal of Engineering and Applied Sciences. ISSN 1819-6608, 9(6): 859-870, EBSCO Publishing, 10 Estes Street, P.O. Box 682, Ipswich, MA 01938, USA.

[14] L. Piancastelli, L. Frizziero, I. Rocchi. 2014. A low-cost, mass-producible, wheeled wind turbine for easy production of renewable energy. Published by Pushpa Publishing House. Far East Journal of Electronics and Communications. ISSN: 0973-7006, 12(1): 19-37, Allahabad, India.

[15] L. Piancastelli, L. Frizziero. 2014. Design, study and optimization of a semiautomatic pasta cooker for coffee shops and the like. Asian Research Publishing Network (ARPN). Journal of Engineering and Applied Sciences. ISSN 1819-6608, 9(12): 2608-2617, EBSCO Publishing, 10 Estes Street, P.O. Box 682, Ipswich, MA 01938, USA.

[16] L. Piancastelli, L. Frizziero, G. Donnici. 2014. Learning by failures: The "Astura II" concept car design process. Asian Research Publishing Network (ARPN). Journal of Engineering and Applied Sciences. ISSN 1819-6608, 9(10): 2009-2015, EBSCO Publishing, 10 Estes Street, P.O. Box 682, Ipswich, MA 01938, USA.

[17] L. Piancastelli, L. Frizziero, T. Bombardi. 2014. Bézier based shape parameterization in high speed mandrel design. International Journal of Heat and Technology, ISSN 0392-8764, 32(1-2): 57-63.

[18] L. Piancastelli, L. Frizziero, 2014. Turbocharging and turbocompounding optimization in automotive racing. Asian Research Publishing Network (ARPN). Journal of Engineering and Applied Sciences. ISSN 1819-6608, 9(11): 2192-2199, EBSCO Publishing, 10 Estes Street, P.O. Box 682, Ipswich, MA 01938, USA.

[19] L. Frizziero, A. Freddi. 2014. Methodology for aesthetical design in a citycar. Asian Research Publishing Network (ARPN). Journal of Engineering and Applied Sciences. ISSN 1819-6608, 9(7): 1064-1068, EBSCO Publishing, 10 Estes Street, P.O. Box 682, Ipswich, MA 01938, USA.

[20] E. Pezzuti, P.P. Valentini, L. Piancastelli, L. Frizziero. 2014. Development of a modular system for drilling aid for the installation of dental implants. Asian Research Publishing Network (ARPN). Journal of Engineering and Applied Sciences. ISSN 1819-6608, 9(9): 1527-1534, EBSCO Publishing, 10 Estes Street, P.O. Box 682, Ipswich, MA 01938, USA.

[21] L. Frizziero. 2014. A coffee machine design project through innovative methods: QFD, value analysis and design for assembly. Asian Research Publishing

Network (ARPN). Journal of Engineering and Applied Sciences. ISSN 1819-6608, 9(7): 1134-1139, EBSCO Publishing, 10 Estes Street, P.O. Box 682, Ipswich, MA 01938, USA.

[22] L. Piancastelli, L. Frizziero, G. Donnici. 2014. Study and optimization of an innovative CVT concept for bikes. Asian Research Publishing Network (ARPN). Journal of Engineering and Applied Sciences. ISSN 1819-6608, 9(8): 1289-1296, EBSCO Publishing, 10 Estes Street, P.O. Box 682, Ipswich, MA 01938, USA.

[23] L. Piancastelli, L. Frizziero, G. Donnici. 2014. The common-rail fuel injection technique in turbocharged di-diesel-engines for aircraft applications. Asian Research Publishing Network (ARPN). Journal of Engineering and Applied Sciences. ISSN 1819-6608, 9(12): 2493-2499, EBSCO Publishing, 10 Estes Street, P.O. Box 682, Ipswich, MA 01938, USA.

[24] L. Piancastelli, L. Frizziero. 2015. Supercharging systems in small aircraft diesel common rail engines derived from the automotive field. Asian Research Publishing Network (ARPN). Journal of Engineering and Applied Sciences. ISSN 1819-6608, 10(1): 20-26, EBSCO Publishing, 10 Estes Street, P.O. Box 682, Ipswich, MA 01938, USA.

[25] L. Piancastelli, L. Frizziero. 2015. Accelerated FEM analysis for critical engine components. Published by Walailak Journal of Science and Technology The Walailak Journal of Science and Technology, Institute of Research and Development, Walailak University, ISSN: 1686-3933, Thasala, Nakhon Si Thammarat 80161. 12(2): 151-165, Thailand.

[26] L. Piancastelli, L. Frizziero, G. Donnici, 2015. Turbomatching of small aircraft diesel common rail engines derived from the automotive field. Asian Research Publishing Network (ARPN). Journal of Engineering and Applied Sciences. ISSN 1819-6608, 10(1): 172-178, EBSCO Publishing, 10 Estes Street, P.O. Box 682, Ipswich, MA 01938, USA.

[27] L. Piancastelli, L. Frizziero. 2015. Multistage turbocharging systems for high altitude flight with common rail diesel engines. Asian Research Publishing Network (ARPN). Journal of Engineering and Applied Sciences. ISSN 1819-6608, 10(1): 370-375, EBSCO Publishing, 10 Estes Street, P.O. Box 682, Ipswich, MA 01938, USA.

[28] L. Piancastelli, L. Frizziero. 2015. A new approach for energy recovery and turbocompounding systems for high altitude flight with common rail diesel engines. Asian Research Publishing Network (ARPN). Journal of Engineering and Applied Sciences. ISSN 1819-6608, 10(2): 828-834, EBSCO Publishing, 10 Estes Street, P.O. Box 682, Ipswich, MA 01938, USA.

[29] L. Piancastelli, L. Frizziero. 2015. Mapping optimization for common rail diesel conversions from the automotive to the flying applications. Asian Research Publishing Network (ARPN). Journal of Engineering and Applied Sciences. ISSN 1819-6608, 10(4): 1539-1547, EBSCO Publishing, 10 Estes Street, P.O. Box 682, Ipswich, MA 01938, USA.

[30] L. Piancastelli, L. Frizziero. 2015. Different approach to robust automatic control for airplanes. Asian Research Publishing Network (ARPN). Journal of Engineering and Applied Sciences. ISSN 1819-6608, 10(6): 2321-2328, EBSCO Publishing, 10 Estes Street, P.O. Box 682, Ipswich, MA 01938, USA.

[31] L. Piancastelli, L. Frizziero. 2015. GA based optimization of the preliminary design of an extremely high pressure centrifugal compressor for a small common rail diesel engine. Asian Research Publishing Network (ARPN). Journal of Engineering and Applied Sciences. ISSN 1819-6608, 10(4): 1623-1630, EBSCO Publishing, 10 Estes Street, P.O. Box 682, Ipswich, MA 01938, USA.

[32] L. Piancastelli, L. Frizziero, G. Donnici. 2015. Common rail diesel - Automotive to aerial vehicle conversions: An update (Part I). Asian Research Publishing Network (ARPN). Journal of Engineering and Applied Sciences. ISSN 1819-6608, 10(6): 2479-2487, EBSCO Publishing, 10 Estes Street, P.O. Box 682, Ipswich, MA 01938, USA.

[33] L. Piancastelli, L. Frizziero, G. Donnici. 2015. Common rail diesel - Automotive to aerial vehicle conversions: An update (Part II). Asian Research Publishing Network (ARPN). Journal of Engineering and Applied Sciences. ISSN 1819-6608, 10(8): 3286-3294, EBSCO Publishing, 10 Estes Street, P.O. Box 682, Ipswich, MA 01938, USA.

[34] L. Piancastelli, L. Frizziero, G. Donnici. 2015. Common rail diesel-electric propulsion for small boats and yachts. Asian Research Publishing Network (ARPN). Journal of Engineering and Applied Sciences. ISSN 1819-6608, 10(6): 2378-2385, EBSCO Publishing, 10 Estes Street, P.O. Box 682, Ipswich, MA 01938, USA.

[35] L. Frizziero, I. Rocchi, G. Donnici, E. Pezzuti, 2015. Aircraft diesel engine turbocompound optimized. JP Journal of Heat and Mass Transfer. ISSN 0973-5763, DOI: 10.17654/JPHMTMay2015_133_150, Volume 11, Issue 2, 1 May 2015, pp. 133-150, Pushpa Publishing House, Vijaya Niwas, 198, Mumfordganj, Allahabad - 211 002, India.

[36] L. Frizziero, L. Piancastelli, 2015. Diesel ecu mapping optimization for aircraft and helicopter applications. JP Journal of Heat and Mass Transfer. ISSN 0973-5763, DOI: 10.17654/JPHMTMay2015_151_167, Volume 11, Issue 2, 1 May 2015, pp. 151-167, Pushpa Publishing House, Vijaya Niwas, 198, Mumfordganj, Allahabad - 211 002, India.